NUMERICAL STUDY ON AERODYNAMIC HEAT OF HYPERSONIC FLIGHT

by

Haiming HUANG [a], Jing XU [a], Weihua XIE [a,b*], and Xiaoliang XU [c]

[a] Institute of Engineering Mechanics, Beijing Jiaotong University, Beijing, China
[b] Center of Composite Materials, Harbin Institute of Technology, Harbin, China
[c] Beijing Institute of Near Space Vehicle's System Engineering, Beijing, China

Original scientific paper
DOI: 10.2298/TSCI1603939H

Accurate prediction of the shock wave has a significant effect on the development of space transportation vehicle or exploration missions. Taking Lobb sphere as the example, the aerodynamic heat of hypersonic flight in different Mach numbers is simulated by the finite volume method. Chemical reactions and non-equilibrium heat are taken into account in this paper, where convective flux of the space term adopts the Roe format, and discretization of the time term is achieved by backward Euler algorithm. The numerical results reveal that thick mesh can lead to accurate prediction, and the thickness of the shock wave decreases as grid number increases. Furthermore, most of kinetic energy converts into internal energy crossing the shock wave.

Key words: *shock wave, aerodynamic heat, finite volume method, Lobb sphere*

Introduction

A very strong shock wave transforms kinetic energy into internal energy when the vehicle flying with high velocity through the atmosphere. The performance of the thermal protection system is critical for aerospace vehicles subjected to aerodynamic heat [1, 2]. The aerodynamic heat loads can be well known from experimental facilities such as wind tunnel and flight experiments, but wind tunnel experiment only simulates part of flight, and flight experiments are too costly to allow their widespread use. Accurate prediction of the aerodynamic heat is badly in need of the development of new vehicle, so the aerodynamic heat of a vehicle during reentry is an open issue of growing interest [3]. A great deal of research has been performed on this subject. For example, Tchuen *et al*. [4] computed the non-equilibrium ionized air flow for a better prediction of hypersonic flows around reentry vehicles. Boyd *et al*. [5] investigated a modified approach for determining the temperature of air with the dissociation and ionization reactions. However, few records have considered the effect of grids on both the thickness of the shock wave and the velocity behind the shock wave. In this study, we will consider thermo-chemical non-equilibrium phenomena of a high temperature gas in order to explore the problem in the aerodynamic heat of hypersonic flight by using the finite volume method.

* Corresponding author; e-mail: michael@hit.edu.cn

Mathematical model

It is well known that the vibration and electron temperatures play an important role in a high temperature gas, because they improve the evaluation of the physical properties of non-equilibrium hypersonic flow. The model of the hypersonic flow with thermal non-equilibrium is built on the basis of aerothermodynamics. The mass conservation equation, the momentum conservation equation and the energy conservation equation of high temperature gas flow are respectively described:

$$\frac{\partial \rho_s}{\partial t} \quad \frac{\partial}{\partial x_j}(\rho_s u_j) \quad \frac{\partial J_{s,j}}{\partial x_j} \quad \omega_s \tag{1}$$

$$\frac{\partial}{\partial t}(\rho_s u_t) \quad \frac{\partial}{\partial x_j}(\rho_s u_i u_j) \quad \frac{\partial}{\partial x_j}[\ P\delta_{ij} \quad \tau_{ij}\ ] \tag{2}$$

$$\frac{\partial E_t}{\partial t} \quad \frac{\partial}{\partial x_j}[(E_t \quad P)u_j\ ] \quad \frac{\partial q_j}{\partial x_j} \quad \frac{\partial}{\partial x_i}(u_j \tau_{ij}) \quad \frac{\partial}{\partial x_j}(\sum_{s\ 1}^{ns} h_s J_{s,j}) \tag{3}$$

$$\rho \qquad \rho_s \tag{4}$$

where ρ, u, P, δ, and τ are the density, velocity, pressure, Kronecker delta function, and shear stress of fluid, respectively. The J is the mass diffusivity flux, ω – the source term associated with the reaction, E – the energy per volume, h – the sensible enthalpy per mass, and q – the heat flux. Subscript s is the species, t is total, i and j are, respectively, i- and j-directions:

$$q_j \qquad \kappa_{\mathrm{tr}} \frac{\partial T}{x_j} \tag{5}$$

where κ is the thermal conductivity, T – the temperature, and subscript tr – the translational-rotational.

The conservation equation for the molecular internal energy is given:

$$\frac{\partial E_{\mathrm{int}}}{\partial t} \quad \frac{\partial}{\partial x_j}(E_{\mathrm{int}} u_j) \quad \frac{\partial}{\partial x_j}(\sum_s e_{\mathrm{int},s} J_{s,j} \quad q_{\mathrm{int},j}) \quad \omega_{\mathrm{int}} \tag{6}$$

$$q_{\mathrm{int},j} \quad \kappa_{\mathrm{int}} \frac{\partial T_{\mathrm{vib}}}{x_j} \tag{7}$$

where e is the molecular energy per mass, subscript int – the internal, and vib – the vibrational. For thermal non-equilibrium, $e_{\mathrm{int},s}$ is defined:

$$e_{\mathrm{int},s} \quad \frac{\mathrm{R}}{M_s} \sum_{m\ 1}^{nd} \frac{g_{s,m}\theta_{s,m}}{(e^{\theta_{s,m}/T_{\mathrm{vib}}} \quad 1)} \tag{8}$$

where R is the universal gas constant, M – the molecular weight, g – the degenerate state, and θ – the characteristic vibrational temperature.

The state equation for gases is given by:

$$P \qquad \sum_s \frac{\rho_s \mathrm{R} T}{M_s} \tag{9}$$

For thermal non-equilibrium:

$$E_t \quad \sum_s \rho_s \ c_{v,\mathrm{tr},s} T \quad \Delta h^0_{f,T_r,s} \quad T_{\mathrm{r}} \ c_{v,\mathrm{tr},s} \quad \frac{\mathrm{R}}{M_s} \qquad E_{\mathrm{int}} \quad \frac{1}{2}\rho u_j u_j \tag{10}$$

where c is the heat capacity, $h^0_{f,T_r,s}$ – the heat of formation at reference temperature, T_r, and pressure for species, s. Subscript v is constant volume:

$$h_s \quad \int_{T_r}^{T} c_{p,\mathrm{tr},s}\mathrm{d}T \quad \Delta h^0_{f,T_r,s} \tag{11}$$

$$c_{v,\mathrm{tr},s} \quad \frac{\varepsilon}{2}\frac{\mathrm{R}}{M_s}, \quad \varepsilon \quad 3,5,6 \tag{12}$$

$$c_{p,\mathrm{tr},s} \quad \frac{\mathrm{R}}{M_s} \tag{13}$$

where ε is the molecular degree of freedom, which has possible values of 3, 5 or 6 for a monatomic species, a diatomic or linear polyatomic species, and a non-linear polyatomic species. Subscript p is a constant pressure.

In addition, the chemical kinetic models for air with seventeen elementary reactions is $O_2 + M = O + O + M$, $N_2 + M = N + N + M$, $NO + M = N + O + M$, $O + N_2 = NO + N$, and $NO + O = O_2 + N$, where the catalytic species M stands for any of the five species.

Results

Roe discrete format is adopted in the discretization of the convection term in this model. Taking Lobb sphere as an example, the aerodynamic heat of hypersonic flight in different Mach numbers (Ma) is simulated by the finite volume method. The Lobb sphere experiment is classic in aerodynamic heat field as it provides many values to compare with. The experimental model is a sphere with radius 6.35 mm. The surface of the Lobb sphere is supposed the no-slip wall and the wall temperature, T_w, is assumed to be a constant. The 5-species-17-reactions chemical reactions come from Park' 85 model [6]. All flow variables are shown in tab. 1.

Table 1. Free stream condition

Altitude [km]	Ma	T [K]	T_w [K]	P [Pa]	Species
35	15.3	293.0	1000	664	79% N_2, 21% O_2

To compare the accuracy, several grids (30×30, 50×50, 70×70, 90×90) are utilized. From fig. 1, the temperature distribution is a basic similarity, and the shock detachment distance is almost the same. They match computational and experimental data in [4], but the thickness of the shock wave decreases as the grid number increases. These results suggest that grids 90×90 is more accurate.

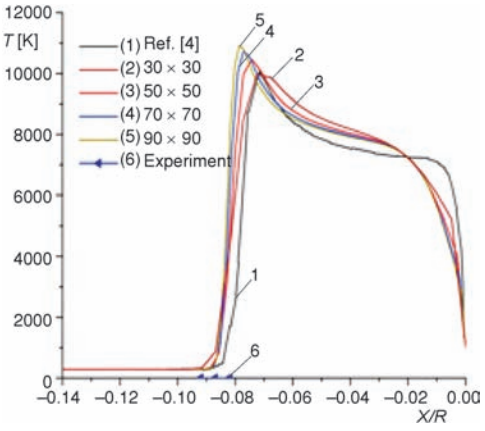

Figure 1. Temperature distributions along the stagnation line

Figure 2 shows that the temperature distributions along the stagnation line are in a good agreement with the data in [4]. The deviations near the wall may be caused by different reaction

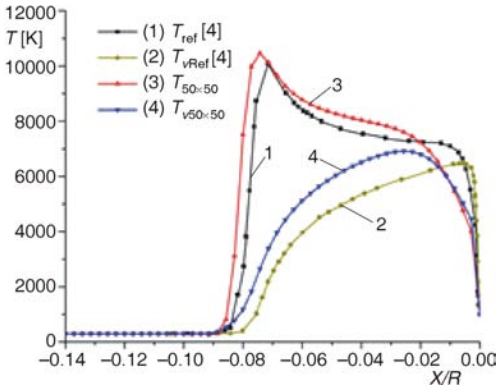

Figure 2. Two-temperature distributions along the stagnation line

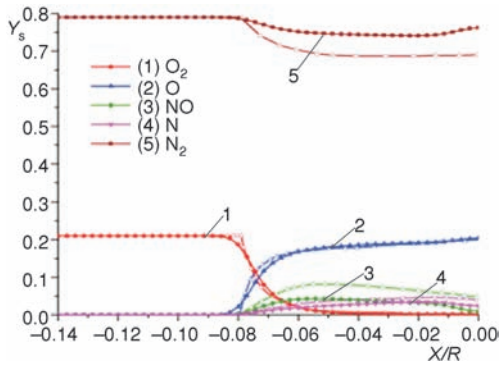

Figure 3. Species mass fractions distributions along the stagnation line

models. The vibrational temperature of the flow field is above 6000 K, so most of O_2 has dissociated but not the N_2.

Species mass fractions distributions along the stagnation line are shown in fig. 3. Lines with solid symbols represent results of this study, and the others represent the results from [4]. As the vibration temperature is not high, N_2 does not dissociate much. Dissociation degree picks up near the wall because the wall temperature is lower than the flow field behind the shock wave. Most of O_2 have dissociated near the wall. Mass fraction of NO peaks after the shock wave but turns to 0 near the wall.

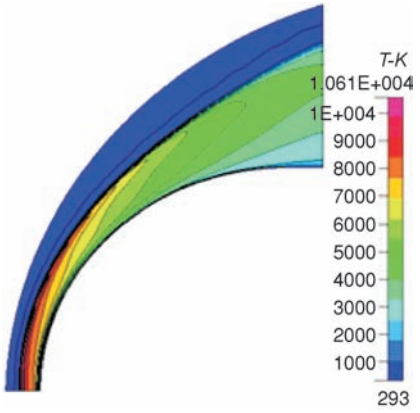

Figure 4. Temperature distribution in the flow field (*for color image see journal web site*)

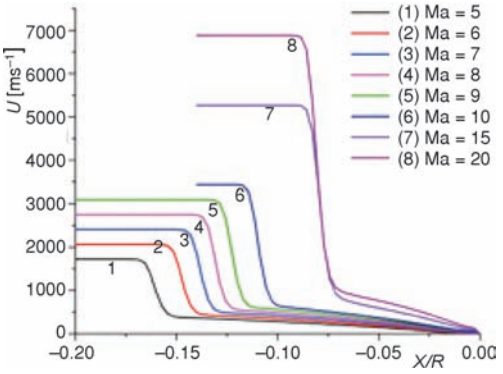

Figure 5. Velocity distributions along the stagnation line with Ma = 5, 6, 7, 8, 9, 10, 15, 20

Temperature distribution in the flow field is illustrated in fig. 4. The peak of temperature is just after the shock wave and then the temperature gradually decreases.

In addition, simulations under several Mach numbers (Ma = 5, 6, 7, 8, 9, 10, 15, and 20) are performed in 50 × 50 grids. Figure 5 shows flow velocity distributions along the stagnation line under different Mach numbers. The shock detachment distance decreases as Mach number increases. Figure 6 shows the relation between the velocities just after shock wave and Mach numbers. The velocity increases as Mach number increases, but not as much as the increment

of flow velocity. These data suggest that most of kinetic energy converts into internal energy crossing the shock wave.

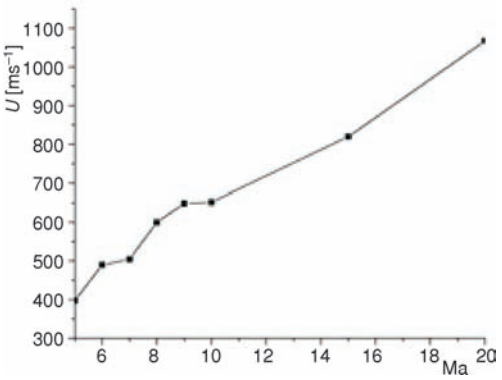

Figure 6. Velocities just after shock wave with Ma = 5, 6, 7, 8, 9, 10, 15, 20

Conclusions

From the numerical results, it can be concluded:

The thickness of the shock decreases as the grid number increases. The more the grid number is, the smaller the thickness of the shock wave becomes.

The shock detachment distance decreases as Mach number increases. However, the velocity just after the shock wave does not increases as much as the increment of flow velocity, which implies that most of kinetic energy converts into internal energy crossing the shock wave.

Acknowledgment

This work is supported by the National Natural Science Foundation of China (Nos. 11472037 and 11272042) and the Project of Education Ministry of China (No.62501036026).

Nomenclature

c – heat capacity, [Jkg^{-1}K^{-1}]
E – energy per volume, [Jkg^{-1}]
e – molecular energy per mass, [Jkg^{-1}]
g – degenerate state, [–]
h – enthalpy per mass, [Jmol^{-1}]
J – mass diffusivity flux, [m^{2}s^{-1}]
M – molecular weight, [kg]
P – pressure, [Pa]
q – heat flux, [Wm^{-2}]
R – universal gas constant
T – temperature, [K]
u – velocity, [ms^{-1}]

Greek symbols

δ – Kronecker delta function, [–]
ε – molecular degree of freedom, [–]
θ – characteristic vibrational temperature, [K]
κ – thermal conductivity, [Wm^{-1}K^{-1}]
ρ – density, [kgm^{-3}]
τ – shear stress, [Pa]
ω – source term, [kgs^{-1}]

Subcripts

i – i-direction
int – inrernal
j – j-direction
p – constant pressure
r – reference
s – species
T_r – reference temperature
t – total
tr – translational-rotational
v – constant volume
vib – vibrational

References

[1] Li, W. J., *et al*, Nonlinear Analysis on Thermal Behavior of Charring Materials with Surface Ablation, *International Journal of Heat and Mass Transfer, 84* (2015), May, pp. 245-252
[2] Li, W. J., *et al.*, A Nonlinear Pyrolysis Layer Model for Analyzing Thermal Behavior of Charring Ablator, *International Journal of Thermal Science, 98* (2015), Dec., pp. 104-112
[3] Li, W. J., *et al*., Thermochemical Ablation of Carbon/Carbon Composites with Nonlinear Thermal Conductivity, *Thermal Science, 18* (2014), 5, pp. 1625-1629
[4] Tchuen, G., *et al*., Numerical Study of Non-Equilibrium Weakly Ionized Air Flow Past Blunt Bodies, *International Journal of Numerical Methods for Heat & Fluid Flow, 15* (2005), 6, pp. 588-610

[5] Boyd, I. D., *et al*., Modeling of Stardust Entry at High Altitude, Part 1: Flowfield Analysis, *Journal of Spacecraft and Rockets, 47* (2010), 5, pp. 708-717
[6] Park, C. A., Review of Reaction Rates in High Temperature Air, *Proceedings*, 24th AIAA Thermophysics Conference, N. Y. USA, 1989

Paper submitted: November 6, 2015
Paper revised: February 1, 2016
Paper accepted: February 21, 2016